PHYSICAL REVIEW A VOLUME 44, NUMBER 6 15 SEPTEMBER 1991

Internal reflection of diffusive light in random media

J.X. Zhu, D.J. Pine, and D.A. Weitz
Exxon Research & Engineering Company, Route 22 East, Annandale, New Jersey 08801
(Received 7 December 1990)

The consequences of internal reflection of multiply scattered light at the boundaries of disordered media are studied. We show that the effect of internal reflection due to index mismatch can be quantitatively accounted for with a single parameter by incorporating a reflection coefficient into the boundary condition for the diffusive light. We measure the angular correlation functions in transmission and reflection at different thicknesses for both high- and low-index mismatch. By including the effect of internal reflection, we are able to obtain consistent quantitative agreement between experiment and theory. Extensions to other experiments including diffusing-wave spectroscopy, coherent backscattering, frequency correlations, and pulse propagation are discussed.

I. INTRODUCTION

The problem of the propagation of light in optically dense random media represents a significant challenge that has attracted considerable attention in recent years [1, 2]. One approach that has met with considerable success is the photon-diffusion approximation. This approximation is valid provided the scattering is not too strong, so that $kl \gg 1$, where l is the scattering mean free path and $k = 2\pi n/\lambda$, with λ the wavelength of the light and n the average index of refraction of the medium. In addition, the diffusion approximation applies only for distances greater than the transport mean free path l^*, the length scale over which the direction of light is randomized by scattering. When these conditions are satisfied, diverse phenomena, such as the spatial and temporal fluctuations of multiply scattered light, pulse propagation, and coherent backscattering, can be understood within this simple, yet powerful framework. While good agreement between experiment and theory is generally achieved, many measurements exhibit systematic deviations from the quantitative predictions of the theory. Recently Lagendijk, Vreeker, and DeVries [3] suggested that the source of these discrepancies may be a failure to properly account for the reflection of light at the boundaries of the random medium. Indeed, by incorporating the effects of internal reflection into the diffusion propagator, they found that internal reflection can lead to significant corrections in the apparent photon diffusion coefficient for pulse propagation through a slab of an optically dense medium. Subsequently, Freund, Rosenbluth, and Berkovits [4] demonstrated that reducing reflections at the sample interface leads to a substantial improvement between experiment and theory for measurements of angular intensity autocorrelation functions. More recently, they used Green's-function methods [5] to show that internal reflection could account for the discrepancies between their earlier reported data and theoretical predictions. Pine *et al.* have also noted that measurements of the temporal correlations of multiple scattered light leads to systematically low estimates of the transport mean free path and have suggested that this may be due to not properly accounting for reflection of light at the sample interface [6, 7].

In this paper, we show that the effects of internal reflection at the boundaries due to index mismatch can be accounted for quantitatively with a single parameter by incorporating a reflection coefficient into the boundary conditions for the diffusion equation for light. We discuss measurements of the decay of the angular correlations in the intensity of multiply scattered light when an optically dense sample is rotated with respect to the incident laser beam. These correlations were first considered by Feng, Kane, and Stone [8] using diagrammatic techniques. Here, we present an alternate theoretical derivation of the correlations using the diffusion equation for light. In addition to being more physically transparent, this approach allows us to incorporate a more realistic treatment of the boundary conditions. By properly accounting for the internal reflection of light in the boundary conditions, we are able to obtain consistent quantitative agreement between experiment and theory for different sample thicknesses and for different index mismatch. An important additional feature of the theory we develop is that it enables us to quantitatively predict value of the reflection coefficient. Exploiting transmission measurements for samples of different thickness, we are able to accurately determine both the internal reflection parameter and the absorption length in the sample. These same parameters can then be used to interpret the angular correlations of backscattered light. In contrast to the transmission measurements, the correlations of the backscattered light are also very sensitive to the nature of the initial conditions which describe the conversion of the incoming plane wave to diffusing light. Here, we obtain good agreement with data by using the rather crude approximation that this conversion occurs at a fixed distance into the sample. An estimate of this distance is obtained from the backscattering results.

The angular correlation of the scattered light upon sample rotation is the simplest of the correlations between incoming and outgoing light described by Feng, Kane, and Stone [8]. These correlations do not depend on any phase interference within the sample, but merely re-

flect the fact that the light propagation is diffusive. As we will show, it is the very simple dependence of the angular correlations on the diffusive propagation that enables us to quantitatively determine the consequences of internal reflection on the boundary conditions. Once these consequences are determined, the new boundary conditions can be used to properly interpret other experiments.

Physically, the consequences of internal reflections can be understood by considering their effect on the distribution of photon path lengths through the sample. The internal reflection due to the mismatch of the index of refraction at the boundary of the random media causes photons to remain inside the medium for a longer time, and thus increases the photon path lengths by an amount determined by the index mismatch. In all backscattering experiments, and in transmission experiments through *thin* samples where path lengths are comparable to l^*, the increase in path length due to internal reflection is generally a significant fraction of the total path length. By contrast, in transmission experiments through *thick* samples, where all paths are long, the increase in path length due to internal reflections is only a small fraction of total path length. Thus the effect of internal reflection is significant for backscattering experiments and transmission experiments through thin samples, and relatively less significant for transmission experiments through very thick samples.

II. THEORY

A. Angular autocorrelation functions

We consider a plane wave that is incident on one side of a slab of random static scatterers. Transmitted or backscattered photons emerge from the sample at a point on the boundary and are detected. The light transport within the sample is assumed to be diffusive and is described by the diffusion equation

$$\frac{\partial U}{\partial t} - D\nabla^2 U = f(t,x,y,z) \ , \tag{2.1}$$

where U is the density of photons, $D = vl^*/3$ is the diffusion coefficient of light, v is the speed of the light inside the sample, and $f(t,x,y,z)$ is the source of diffusing light. The path of each diffusing photon is determined by random multiple scattering from a sequence of scatterers. The multiply scattered electrical field E emerging from the sample is made up of the contributions of fields following many different scattering paths

$$E = \sum_p E_p \ , \tag{2.2}$$

where p denotes a scattering path. The scattering intensity is given by

$$I = \sum_{p,p'} E_p E_{p'}^* \ . \tag{2.3}$$

Rotating the sample changes the relative phase of the field between paths and, as a result, the scattered intensity fluctuates. The ensemble-averaged intensity is given by

$$\langle I \rangle = \sum_{p,p'} \langle E_p E_{p'}^* \rangle = \sum_p \langle E_p E_p^* \rangle \ . \tag{2.4}$$

The second equality follows from our assumption that the positions of scatterers are randomly distributed and that the relative phases of fields from different paths are uncorrelated and therefore average to zero; the only nonvanishing terms in $\langle E_p E_{p'}^* \rangle$ are those with $p = p'$, where the random phases of fields are canceled by their conjugates. We measure the intensity correlation of backscattered or transmitted light as the sample is rotated along an axis normal to the direction of the incident light. The autocorrelation function is defined as

$$G_2(\theta) \equiv \langle I(0) I(\theta) \rangle = \sum_{p,p',p'',p'''} \langle E_p(0) E_{p'}^*(0) E_{p''}(\theta) E_{p'''}^*(\theta) \rangle \ , \tag{2.5}$$

where θ is the angle rotated and $I(\theta)$ the intensity of the light. Once again, because the relative phases of fields are random, the leading nonzero terms are those with $p = p'$ and $p'' = p'''$ or $p = p'''$ and $p' = p''$. Then Eq. (2.5) factorizes:

$$G_2(\theta) = \sum_{p,p',p'',p'''} \langle E_p(0) E_{p'}^*(0) \rangle \delta_{p,p'} \langle E_{p''}(\theta) E_{p'''}^*(\theta) \rangle \delta_{p'',p'''} + \sum_{p,p',p'',p'''} \langle E_p(0) E_{p'''}^*(\theta) \rangle \delta_{p,p'''} \langle E_{p'}^*(0) E_{p''}(\theta) \rangle \delta_{p',p''} = \langle I \rangle^2 + \left| \sum_p \langle E_p(0) E_p^*(\theta) \rangle \right|^2 \tag{2.6}$$

For later use, we define

$$g_2(\theta) \equiv \frac{G_2(\theta)}{\langle I \rangle^2} - 1 \tag{2.7}$$

and

$$g_1(\theta) \equiv \frac{\sum_p \langle E_p(0) E_p^*(\theta) \rangle}{\langle I \rangle} \ . \tag{2.8}$$

From Eq. (2.6), we see that $g_2(\theta)$ and $g_1(\theta)$ are related:

$$g_2(\theta) = |g_1(\theta)|^2 \ . \tag{2.9}$$

This equation, known as the Siegert relation, allows us to obtain intensity correlation functions from calculations of the field correlation functions. Thus, in subsequent sec-

tions we always calculate the field correlation functions and use Eq. (2.9) to obtain intensity correlation functions for comparison with our experiments.

To calculate these autocorrelation functions we first determine the contribution of a single diffusive light path due to the rotation of the sample. This corresponds to calculating the argument of the summation in Eq. (2.8). Then the contributions of all paths, weighted by the distribution of the paths, are summed to obtain the desired correlation function. The photon path distributions for transmission and backscattering geometries can be determined by solving the diffusion equation *provided one uses boundary conditions which properly account for the behavior of the light at the sample interfaces.* In the following section, we discuss the behavior of light near interfaces and develop boundary conditions which account for the effect of internal reflection at the sample interfaces. We then use these results to obtain explicit expressions for the angular correlation functions of multiply scattered light. These results are compared with experiments and then generalized to several other types of measurements involving strong multiple scattering. We show that the simple angular correlation measurements allow the determination of the parameters that characterize the effects of internal reflection. These parameters can then be used directly to account for the effects of internal reflection in other measurements.

B. Internal reflections and boundary conditions

A variety of boundary conditions have been used to describe the behavior of diffusing light at a sample interface. The simplest approach is to use perfectly absorbing boundary conditions $U=0$. Feng, Kane, and Stone [8] have used these boundary conditions within a diagrammatic expansion to obtain an expression for the angular correlation function for transmission through a slab of thickness L. They obtain

$$g_1(\theta) = \frac{k_0 \theta L}{\sinh(k_0 \theta L)} , \tag{2.10}$$

where $k = 2\pi/\lambda$. However, perfectly absorbing boundary conditions are known to be inconsistent with the exact Milne solution for scattering from uncorrelated point particles [1]. Furthermore, because perfectly absorbing boundary conditions cannot account for internal reflection of light at the interfaces, Eq. (2.10) fails to quantitatively describe the experimental results [4]. Thus more accurate boundary conditions are required.

To obtain more realistic boundary conditions, we consider the flux of diffusing photons scattered through an arbitrary small area dS *inside the sample.* For simplicity, we will assume that the sample is made up of isotropic scatterers and that absorption can be neglected (these assumptions will be relaxed later). Without loss of generality, we let dS be at the origin and perpendicular to z axis, as shown in Fig. 1. The flux of photons scattered directly from the volume element dV through dS is given by the product of the number of photons in dV, $U(r,\theta,\varphi)dV$, the fractional solid angle $\cos\theta dS/r^2$, the speed of light v, and the loss due to the scattering between dV and dS, $\exp(-r/l)$:

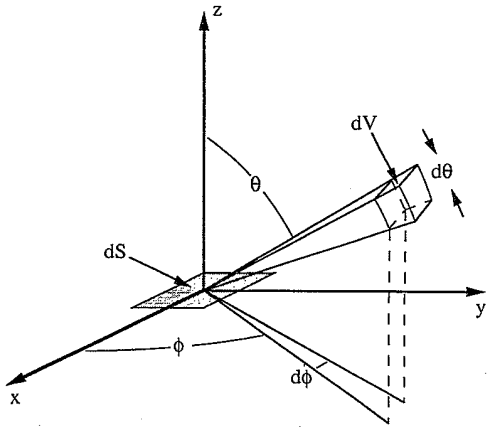

FIG. 1. Scattering geometry for the calculation of the photon flux.

$$U(r,\theta,\varphi)dV v \frac{\cos\theta dS}{r^2} e^{-r/l} . \tag{2.11}$$

Replacing dV by $r^2 \sin\theta dr d\theta d\varphi$, this can be rewritten as

$$\frac{dS}{4\pi} U(r,\theta,\varphi) v \cos\theta \sin\theta e^{-r/l} dr d\theta d\varphi . \tag{2.12}$$

The total flux of photons scattered into the area dS per unit time in the negative z direction is obtained by integrating over the number coming from the entire half-space $z > 0$. Denoting the photon flux in the $-z$ direction as J_-, we have

$$J_- dS = \frac{dS}{4\pi} v \int_0^{\pi/2} d\theta \int_0^{2\pi} d\varphi \int_0^{\infty} dr\, U(r,\theta,\varphi) \times \cos\theta \sin\theta e^{-r/l} . \tag{2.13}$$

To evaluate this integral, we expand $U(r,\theta,\varphi)$ about the origin. Since the primary contribution to the photon flux through dS is from the neighborhood of a few mean free paths away, we can restrict the expansion to first-order terms in a Taylor expansion,

$$U(r,\theta,\varphi) = U_0 + x\left(\frac{\partial U}{\partial x}\right)_0 + y\left(\frac{\partial U}{\partial y}\right)_0 + z\left(\frac{\partial U}{\partial z}\right)_0 , \tag{2.14}$$

where the derivatives are to be evaluated at the origin. The independent variables x, y, and z may be expressed in terms of spherical coordinates by

$$\begin{aligned} x &= r\sin\theta\cos\varphi , \\ y &= r\sin\theta\sin\varphi , \\ z &= r\cos\theta . \end{aligned} \tag{2.15}$$

Since the integration over φ in Eq. (2.13) is between the limits of zero and 2π, the terms containing x and y will make no net contribution. Thus, replacing z by $r\cos\theta$ and integrating over r and φ, we obtain

$$J_- = \frac{v}{4\pi}\int_0^{\pi/2} d\theta \int_0^{2\pi} d\varphi \int_0^{\infty} dr \left(U + r\frac{\partial U}{\partial z}\cos\theta\right) \times \cos\theta \sin\theta e^{-r/l}$$
$$= \frac{Uv}{4} + \frac{D}{2}\left(\frac{\partial U}{\partial z}\right) , \quad (2.16)$$

where $D = vl/3$ is the diffusion coefficient of light and, for convenience, we neglect the subscript zero. Similarly the photon flux through dS in z direction, J_+, may be obtained by integrating the contributions from $z < 0$:

$$J_+ = \frac{v}{4\pi}\int_{-\pi/2}^{0} d\theta \int_0^{2\pi} d\varphi \int_0^{\infty} dr \left(U + r\frac{\partial U}{\partial z}\cos\theta\right) \times \cos\theta \sin\theta e^{-r/l}$$
$$= \frac{Uv}{4} - \frac{D}{2}\left(\frac{\partial U}{\partial z}\right) . \quad (2.17)$$

Equations (2.16) and (2.17) can be generalized to treat the anisotropic scatterers typically used in experiments. Here the single-particle scattering is peaked in the forward direction so that the effective random-walk step size is the transport mean free path l^*, where l^* is defined by the relation $l/l^* = \langle 1 - \cos\theta \rangle$. It can be shown [9] that Eqs. (2.16) and (2.17) are satisfactory for anisotropic systems, provided that l^* replaces l in the definition of the diffusion coefficient, i.e., $D = vl^*/3$.

Now consider the photon flux at the boundaries at z=0 and L. If there is no internal reflection, there will be no photon flux from outside the sample, that is, J_+=0 at z=0 and J_- =0 at $z = L$. This gives the mixed boundary conditions

$$U - \frac{2l^*}{3}\frac{\partial U}{\partial z} = 0 \quad \text{at } z = 0 , \quad (2.18)$$
$$U + \frac{2l^*}{3}\frac{\partial U}{\partial z} = 0 \quad \text{at } z = L . \quad (2.19)$$

By contrast, if there is internal reflection, there will be some incoming flux due to the reflection at the boundaries. The simplest treatment is to define a reflection coefficient R, which is the ratio of the incoming flux to the outgoing flux at the boundaries. Thus the boundary conditions are $J_+ = RJ_-$ for $z = 0$ and $J_- = RJ_+$ for $z = L$. This gives boundary conditions

$$U - C\frac{\partial U}{\partial z} = 0 \quad \text{at } z = 0 , \quad (2.20)$$
$$U + C\frac{\partial U}{\partial z} = 0 \quad \text{at } z = L , \quad (2.21)$$

where

$$C \equiv \frac{2l^*}{3}\frac{1+R}{1-R} . \quad (2.22)$$

When R=0, we recover the mixed boundary conditions for no reflections. If we assume $\partial U/\partial z$ is constant inside the sample near the boundaries, Eqs. (2.20) and (2.21) are essentially equivalent to extrapolating U to 0 at a distance C outside of the boundaries. In the limit that $R = 0$, $C = 2l^*/3$, which is very near the frequently used extrapolation length of $0.7104l^*$ given by the Milne solution [1]. However, in the presence of reflections, this extrapolation length can be significantly larger.

C. Calculation of angular correlation functions

For convenience, we assume that the incident light is at near normal incidence on a slab of thickness L and that the wave vector of the detected light is approximately parallel to the incident light. As shown in Fig. 2, we define a coordinate system with an origin on one side of the sample where the light is incident at $z = 0$ from the $-z$ direction. The sample is rotated about the x axis. A typical diffusing-light path through the sample is also shown in Fig. 2. A photon incident on the slab at a position $\mathbf{r}_i = (x_i, y_i, 0)$ follows a path of total length s through the sample and emerges at a position $\mathbf{r}_t = (x_t, y_t, L)$. We calculate the phase shift of photons traversing this same path after the sample rotates through a small angle θ. The phase shift arises from the change in the *total* length of this path. However, since the scatterers are stationary, the path length *within* the sample is unchanged upon rotation, and all the phase shift arises from the change in path length *outside* the sample. As shown in Fig. 2, there are two contributions to the change in path length, one from each side of the sample. The path length of the incident light is decreased by $y_i\theta$, while that of the emerging light is decreased by $y_t\theta$. Defining a scattering wave vector $q = k_0\theta$, the total phase difference of the path on rotation is $\Delta\phi_T = \Delta\phi_i + \Delta\phi_t = q(y_t - y_i) + O(\theta^2)$. Thus, if the electric field at $\mathbf{r}_t$ is initially $E(0)$, then after the sample is rotated through an angle θ, the electric field will be

$$E(\theta) = E(0)e^{iq(y_t - y_i)} . \quad (2.23)$$

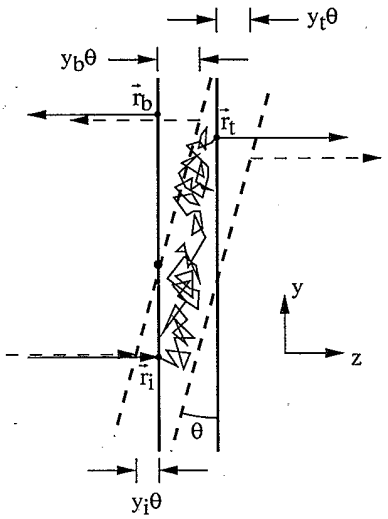

FIG. 2. Experimental geometry with a typical diffusive light path shown. The input, transmission output, and backscattering output points $\mathbf{r}_i$, $\mathbf{r}_t$, and $\mathbf{r}_b$, respectively, are shown in their initial positions. The dashed lines indicate the sample position after the sample is rotated through an angle θ.

Photons incident at $\mathbf{r}_i$ can travel many different paths within the sample before emerging at $\mathbf{r}_t$. We denote by $p(s,\mathbf{r}_i,\mathbf{r}_t)$ the probability that, in the absence of absorption, a photon follows a path of length s whose end points are at $\mathbf{r}_i$ and $\mathbf{r}_t$. Since the light emerging at any single point from the sample is made up of contributions of different paths beginning anywhere on the incident face of the slab, we can calculate the angular correlation function of the electric field by summing over all paths and all incident points:

$$g_1(q) \equiv \frac{\langle E(0)E^*(\theta)\rangle}{\langle E(0)E^*(0)\rangle} \tag{2.24}$$

$$\simeq \int ds\, dx_i\, dy_i\, p(s,\mathbf{r}_i,\mathbf{r}_t)\, e^{iq(y_t-y_i)} e^{-s/l_a}\,, \tag{2.25}$$

where we have also accounted for the possibility of absorption by including an exponential cutoff with an absorption length l_a. Similarly, we can calculate the phase shift for a backscattered photon following the path shown in Fig. 2 and emerging at a posititon on the incident face $\mathbf{r}_t = (x_t, y_t, L)$. For this case, we obtain $\Delta\phi_B = \Delta\phi_b + \Delta\phi_i = q(y_b + y_i) + O(\theta^3)$. The angular autocorrelation function of backscattered fields is then given by

$$g_1(q) \simeq \int ds\, dx_i\, dy_i\, p(s,\mathbf{r}_i,\mathbf{r}_b)\, e^{iq(y_b+y_i)} e^{-s/l_a}\,. \tag{2.26}$$

In addition to collecting light from a single point on the outgoing surface as discussed above, it is also instructive to consider collecting the light from the whole outgoing plane. This entails an additional integration over the outgoing surface to calculate the correlation function. However, the results can be seen immediately from symmetry arguments. For transmission, the phase shift depends only on the difference $y_t - y_i$ and thus $g_1(q)$ is translationally invariant on the outgoing plane. Thus summing over the whole plane yields the same result as for a point. By contrast, for backscattering the phase shift depends on the sum $y_b + y_i$. Thus $g_1(q)$ is not translationally invariant on the outgoing plane. In this case summing over the plane results in no correlations at all.

To obtain explicit expressions for $g_1(q)$ from Eqs. (2.25) and (2.26), we must determine $p(s,\mathbf{r}_i,\mathbf{r}_b)$ for each scattering geometry. To this end, we consider an instantaneous pulse of light which begins to diffuse a distance z_0 inside the slab at $t = 0$, so that the initial conditions for the diffusion equation are

$$f(t,x,y,z) = \delta(t)\delta(x-x_i)\delta(y-y_i)\delta(z-z_0), \tag{2.27}$$

where we expect $z_0 \simeq l^*$. Photons emerging at $\mathbf{r}_t$ at time t have all traveled a distance $s = vt$. The average number (or flux) of photons emerging from the sample at $\mathbf{r}_t$ at time t will be proportional to the probability that a photon travels a distance s from $\mathbf{r}_i$ to $\mathbf{r}_t$, that is, $p(s,\mathbf{r}_i,\mathbf{r}_t)$. The photon flux can be determined within the diffusion approximation by solving the diffusion equation, Eq. (2.1), for U, subject to the appropriate boundary conditions for U at $z = 0$ and L, and then calculating the outward flux at the boundaries using Eqs. (2.16) or (2.17). The solution of Eq. (2.1) can be simplified by separating U into three parts,

$$U(x,y,z,t) = X(x,t)Y(y,t)Z(z,t)\,, \tag{2.28}$$

where

$$X(x,t) = \frac{1}{\sqrt{4\pi Dt}} \exp\left(-\frac{(x-x_i)^2}{4Dt}\right)$$

and

$$Y(y,t) = \frac{1}{\sqrt{4\pi Dt}} \exp\left(-\frac{(y-y_i)^2}{4Dt}\right)$$

are the solutions to the one-dimensional diffusion equations $\partial X/\partial t - D\nabla^2 X = \delta(x-x_i)\delta(t)$ and $\partial Y/\partial t - D\nabla^2 Y = \delta(y-y_i)\delta(t)$ in an infinite medium, and $Z(z,t)$ is the solution to the equation

$$\partial Z/\partial t - D\nabla^2 Z = \delta(z-z_0)\delta(t)\,, \tag{2.29}$$

subject to the boundary conditions

$$Z - C\frac{\partial Z}{\partial z} = 0 \quad \text{at } z = 0\,, \tag{2.30}$$

$$Z + C\frac{\partial Z}{\partial z} = 0 \quad \text{at } z = L\,. \tag{2.31}$$

The transmitted flux from the sample at $\mathbf{r}_t$ is

$$J_+ = \frac{Uv}{4} - \frac{D}{2}\frac{\partial U}{\partial z}$$

$$= \frac{Uv}{2(1+R)} = \frac{vXYZ}{2(1+R)} \quad \text{at } z = L\,, \tag{2.32}$$

where the second equality follows from the boundary condition at $z = L$, Eq. (2.21). Similarly, the backscattered flux from the sample at $\mathbf{r}_b$ is

$$J_- = \frac{Uv}{4} + \frac{D}{2}\frac{\partial U}{\partial z}$$

$$= \frac{Uv}{2(1+R)} = \frac{vXYZ}{2(1+R)} \quad \text{at } z = 0\,. \tag{2.33}$$

Equations (2.32) and (2.33) are directly proportional to $p(s,\mathbf{r}_i,\mathbf{r}_t)$ and $p(s,\mathbf{r}_i,\mathbf{r}_b)$, respectively, when the time dependence t in XYZ is replaced by s/v. Substituting these expressions for $p(s,\mathbf{r}_i,\mathbf{r}_t)$ and $p(s,\mathbf{r}_i,\mathbf{r}_t)$ into Eqs. (2.25) and (2.26), and then integrating over x_i and y_i, we obtain

$$g_1(q) \propto \int_0^\infty P(s) e^{-(q^2+\alpha^2)l^* s/3} ds\,, \tag{2.34}$$

where $\alpha^2 \equiv 3/l^* l_a$ and $P(s) \propto Z(z,t)|_{z=L}$ for transmission and $P(s) \propto Z(z,t)|_{z=0}$ for backscattering where, once again, we use the transformation $t = s/v$. That is, $P(s)$ is proportional to the solution of the one-dimensional diffusion equation, Eq. (2.29), and thus is the probability of a photon having a path length s regardless of its end points. From Eq. (2.34), we see that paths with large s decay more rapidly than paths with small s. Physically, this is because paths with large s

have, on average, a larger transverse separation $y_t - y_i$ or $y_b - y_i$ of their end points. This larger separation results in a larger change in phase when the sample is rotated, as can be seen from the expression for the θ dependence of the electric field, Eq. (2.23). We note here, and we will discuss in more detail later, that Eq. (2.34) has, apart from a simple transformation of variables, the same form as the expressions for the coherent backscattering cone and the temporal autocorrelation function. This is due to the fact that all these effects depend on changes in the phase of the multiply scattered light which scale linearly with the path length s.

The calculation of $g_1(q)$ can be further simplified by noting that Eq. (2.34) is the Laplace transform of $P(s)$. Thus, instead of solving the diffusion equation to obtain $P(s)$, we can solve the Laplace transform of the one-dimensional diffusion equation, Eq. (2.29), and obtain $g_1(q)$ directly. The solution of the diffusion equation using the Laplace transform is given in Carslaw and Jaeger for this slab geometry [10]. They obtain

$$\bar{Z} = \int_0^\infty Z(z,t)e^{-pt}dt = \frac{1}{2D\eta^2}e^{-\eta|z-z_0|} + A\sinh(\eta z) + B\cosh(\eta z)\ , \quad (2.35)$$

where $\eta = \sqrt{p/D}$ and the coefficients A and B are chosen so that the boundary conditions, the Laplace tranformations of Eqs. (2.30) and (2.31), are satisfied at $z = 0$ and L, respectively. After tedious but straightforward algebra, we obtain

$$\bar{Z} = \frac{\sinh[(L - z + z_0)\eta] + Cp\cosh[(L - z + z_0)\eta]}{(1 + C^2\eta^2)\sinh(L\eta) + 2C\eta\cosh(L\eta)}\ . \quad (2.36)$$

Comparing Eqs. (2.34) and (2.35), we see that $\bar{Z}$ is equivalent to $g_1(q)$ if one makes the transformation of variables $s \to t/c$ and $p = D\eta^2 \to (q^2 + \alpha^2)vl^*/3$. The second transformation is equivalent to $\eta \to \sqrt{q^2 + \alpha^2}$. Thus, in transmission, where $z = L$, we obtain

$$g_1(q) = \frac{(L + 2C)/(z_0 + C)[\sinh(z_0\sqrt{q^2+\alpha^2}) + C\sqrt{q^2+\alpha^2}\cosh(z_0\sqrt{q^2+\alpha^2})]}{[1 + C^2(q^2+\alpha^2)]\sinh(L\sqrt{q^2+\alpha^2}) + 2C\sqrt{q^2+\alpha^2}\cosh(L\sqrt{q^2+\alpha^2})}\ . \quad (2.37)$$

For $z_0/L \ll 1$, $g_1(q)$ is insensitive to the exact value of z_0. Physically, this means that for light transmission through thick samples, the exact depth into the sample at which the light begins to diffuse is unimportant. For perfectly absorbing boundary conditions ($C = 0$), Eq. (2.37) reduces to Eq. (2.10), $g_1(q) = qL/\sinh(qL)$, derived by Feng, Kane and Stone, provided there is no absorption ($\alpha = 0$) and the sample is very thick ($z_0/L \ll 1$).

For $C/L \ll 1$, Eq. (2.37) is equivalent to the results of Feng, Kane, and Stone, but for a sample with an effective thickness of $L + 2C$ rather than L. Thus the effect of reflections is to increase the apparent thickness of the sample. To see this, we consider a sample with an effective thickness of $L + 2C$. We use the simple boundary conditions $U = 0$ at $z = -C$ and $L + C$, and evaluate $g_1(q)$ at $z = L$. We obtain

$$g_1(q) \propto \frac{\sinh[(z + 2C)\sqrt{q^2+\alpha^2}] + \sinh(z_0\sqrt{q^2+\alpha^2})}{\sinh[(L + 2C)\sqrt{q^2+\alpha^2}]}\ . \quad (2.38)$$

In the case of $C/L \ll 1$, we can make the approximations $\sinh(2Cq) \simeq 2Cq$ and $\cosh(2Cq) \simeq 1 + 2C^2q^2$, to obtain

$$g_1(q) \propto \frac{[1 + C^2(q^2+\alpha^2)]\sinh(z_0\sqrt{q^2+\alpha^2}) + C\sqrt{q^2+\alpha^2}\cosh(z_0\sqrt{q^2+\alpha^2})}{[1 + 2C^2(q^2+\alpha^2)]\sinh(L\sqrt{q^2+\alpha^2}) + 2C\sqrt{q^2+\alpha^2}\cosh(L\sqrt{q^2+\alpha^2})}\ . \quad (2.39)$$

Equations (2.37) and (2.39) are identical if we neglect terms with C^2. This calculation also suggests that the effects of internal reflection become less important for thick samples.

In contrast to transmission, the diffusion equation does not fully describe backscattered light because it consists of a significant contribution of paths of length comparable to the transport mean free path. However, Pine *et al.* [11] have shown that the diffusion equation can provide a surprisingly accurate description of temporal correlation functions of backscattered light with the boundary condition $U = 0$ provided that the incident light is artificially assumed to start diffusing at a fixed distance γl^* inside the sample. The parameter γ then appears in their expression for the correlation function as the initial slope of the decay. Caution must be excised in assigning a physical meaning to γ since it is observed to depend on the polarization of the incident and detected light and on the ratio of the transport and scattering mean free paths [12]. Here we show that the initial slope is also a function of the internal reflection.

To obtain an expression for the angular correlation in backscattering we let $z = 0$ in Eq. (2.36) and obtain

$$g_1(q) \propto \frac{\sinh[(L - z_0)\sqrt{q^2+\alpha^2}] + C\sqrt{q^2+\alpha^2}\cosh[(L - z_0)\sqrt{q^2+\alpha^2}]}{[1 + C^2(q^2+\alpha^2)]\sinh(L\sqrt{q^2+\alpha^2}) + 2C\sqrt{q^2+\alpha^2}\cosh(L\sqrt{q^2+\alpha^2})}\ . \quad (2.40)$$

For thick samples, where $L/z_0 \gg 1$ and $L/C \gg 1$, Eq. (2.40) becomes

$$g_1(q) \propto \frac{\exp(-z_0\sqrt{q^2+\alpha^2})}{1+C\sqrt{q^2+\alpha^2}} . \quad (2.41)$$

In the case of weak absorption $\alpha \ll q$, the initial decay of Eq. (2.41) can be approximated by

$$g_1(q) = 1-(z_0+C)q = 1-(z_0+C)k_0\theta . \quad (2.42)$$

Here, the initial slope, $dg_1/d\theta = [z_0/l^* + \frac{2(1+R)}{3(1-R)}]k_0 l^*$ depends critically on the internal reflection.

Internal reflection increases the photon path lengths and causes $g_1(q)$ to decay more rapidly. By contrast, absorption cuts off long paths and causes $g_1(q)$ to decay more slowly. We can exploit this fact to experimentally determine both α and C by making measurements in transmission as a function of sample thickness. For a thin sample, where $\alpha L \ll 1$, $g_1(q)$ depends only on the sample thickness and the internal reflection, that is, on L and C. By contrast, for a thick sample, where $C/L \ll 1$, the effect of internal reflection becomes small and $g_1(q)$ only depends on the sample thickness and the absorption, that is, on L and α. Thus, by measuring $g_1(q)$ in transmission and backscattering for different thicknesses, we can determine C and α. These quantities can then be used to interpret other phenomena involving multiple light scattering, such as frequency correlation and pulse propagation. We will show that the theory is in good agreement with our experiments for samples with both large and small index mismatch, in both transmission and backscattering geometries, and for several different sample thicknesses.

III. EXPERIMENT

A. Samples and procedure

In our experiment we use two sets of samples, one of which has a higher average index of refraction than the other. The first set is made of sintered polydisperse alumina particles with a mean diameter of about 2.5 μm and a volume fraction of 0.96. Three samples with thicknesses of 0.615, 0.385, and 0.256 mm were used. The second set is from commercial glass frits with pore sizes between 10 and 20 μm and with a volume fraction of glass of approximately 0.96. The index of refraction of solid alumina is 1.7, while that of glass is 1.5. Thus we expect that the effect of internal reflection should be stronger for the higher-index alumina samples than for the lower-index glass frit sample.

The samples were mounted on a vertical translation stage and placed at the center of a rotation stage. We used the 488-nm line of an Ar^+ laser; the beam was expanded to a diameter of 1 cm, collimated, and then directed towards the sample at near-normal incidence. Two methods were used to collect the scattered light in transmission or backscattering. In the first method, we measured the scattered intensity at a single point near the center of the sample, which was aligned to be on the axis of rotation. This central spot was imaged one to one onto a 25-μm pin hole with a 50-cm focal length lens. A 4.3-mm aperture was placed in front of the lens to determine the angular width of the detected light and to ensure that only a single speckle spot, and thus a single wave vector, was detected. In the second method, we measured all the transmitted or backscattered light with the wave vector the same or opposite to that of the incident wave vector. This was accomplished by placing the detector pin hole at the focal plane of the collection lens. To accumulate the autocorrelation function, the sample was rotated about the center of the incident beam. It was turned from 85 to 95 deg relative to the incident beam at a constant angular speed of $\omega = 5 \times 10^{-2}$ deg per sec. The scattered intensity was detected with a photomultiplier tube using photon counting electronics. A digital correlator was used to measure the temporal intensity correlation function. The temporal intensity correlation function was converted to $g_2(q)$ using the relation $\theta = \omega t$. To ensure good ensemble averaging, we averaged several runs illuminating different areas of the samples.

From the correlator, we obtain normalized intensity correlation functions $\langle I(0)I(q)\rangle/\langle I\rangle^2 = 1+\beta g_2(\theta)$, where β is a constant of order unity which is determined by the number of speckle spots detected. Our detection area was about half a speckle spot, corresponding to $\beta \simeq 0.8$.

B. Results

In Fig. 3, we plot the normalized angular intensity autocorrelation functions obtained from a 0.385-mm-thick alumina sample. Angular correlation functions obtained in the transmission geometry are shown in Fig. 3(a) for the two cases of planar and point collection optics. They are identical to within experimental uncertainty. This reflects the vertical (y-direction) translational invariance of the expression for the change in phase, Eq. (2.25), for each light path upon sample rotation. By contrast, angular correlation functions obtained in the backscattering geometry decay very differently for planar and point collection optics, as shown in Fig. 3. The dashed curve in

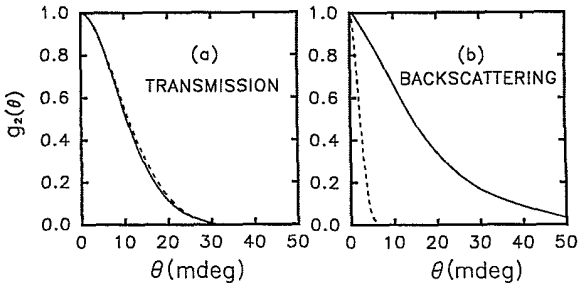

FIG. 3. Comparison of angular correlation functions obtained using planar (dashed lines) and point (solid lines) collection optics. (a) For the transmission geometry, the decay of $g_2(\theta)$ is independent of the collection optics. (b) For the backscattering geometry, the decay of $g_2(\theta)$ is much more rapid for planar detection optics than for point detection optics.

Fig. 3(b) was obtained by collecting light over the entire outgoing plane, an area approximately 1 cm in diameter. The dashed curve decays much more rapidly than the solid curve, which was obtained by collecting light from a single point. In fact, the residual correlation in the dashed curve reflects only the finite size of the collection optics and the resultant finite speckle size. Thus the absence of translational invariance over the collection plane in the backscattering geometry results in drastically different correlation functions, depending on whether planar or point collection optics are used while in transmission; the translational invariance ensures that the two collection schemes yield identical results. In the remainder of this paper we report only measurements obtained using point collection optics.

In Fig. 4, we show autocorrelation functions obtained in the transmission geometry for alumina samples of three different thicknesses. As expected, the autocorrelation functions decay more rapidly with increasing sample thickness. This reflects the fact that longer paths dephase the light more rapidly than do shorter paths. The solid lines are fits to the data using Eq. (2.37) with a single set of fitting parameters: $C = 0.212$ mm and $\alpha = 0.8$ mm^{-1} for all three samples. The fact that a single set of parameters describe the data for all three samples strongly supports the theory developed in Sec. II. For comparison we also show, by the dashed line, the result of the theory for the thickest ($L = 0.615$ mm) sample with $C = 0$ and $\alpha = 0$, i.e., without any internal reflection or absorption. The disagreement between these calculations and the measurements is apparent. It is important to note that increasing internal reflection tends to move the dashed curve towards the data and improve the agreement between theory and experiment, while increasing absorption tends to move the dashed curve away from the data. Physically, this follows from the fact that internal reflection increases the effective length of the light paths through the sample, while absorption tends to attenuate the contribution of the longer paths. Thus it is the inclusion of reflection in the theory which provides the improved agreement with the data.

To better appreciate the relationship between $g_2(q)$ and L we plot the half-width θ_h of the measured autocorrelation functions as L is varied. The values for the alumina samples are shown in Fig. 5(a). The lower solid line through the data is a fit to Eq. (2.37) and is in excellent agreement with experimental data. From the fit we obtain $C = 0.212 \pm 0.001$ mm and $\alpha = 0.8 \pm 0.1$ mm^{-1}, in excellent agreement with the values obtained from the fit to the individual autocorrelation functions. The dashed line is calculated from Eq. (2.10), without the effect of internal reflection and absorption, and cannot account for the observed behavior. The internal reflection has the strongest effect for those samples with the highest index mismatch, particularly the thinnest samples. Since the thinnest samples have the shortest characteristic photon path lengths without internal reflection, the fractional increase in path length due to internal reflection is greatest in these samples. In Fig. 5(b), we plot θ_h for the glass frit samples and fit the data with Eq. (2.37) to obtain $C = 0.143 \pm 0.001$ mm and $\alpha = 0.5 \pm 0.1$ mm^{-1}. Again, the agreement between theory and experiment is excellent. Furthermore, the effect of the internal reflection is considerably less for these samples since their index mismatch is less. In fact, for the thickest sample $L = 2.92$ mm the effect of the internal reflection is negligible. Nevertheless, over the full range of sample thicknesses used, inclusion of internal reflection in the theory provides substantially better agreement with the data than the theory with $C = 0$, which is shown by the dashed curve in Fig. 5(b).

In order to determine the reflection coefficient R from our measurements of C, we must know l^* for our samples. We can obtain a good estimate of l^* by combining our measurements of $g_2(\theta)$ in transmission with measurements of $g_2(\theta)$ in backscattering. In backscattering, the angular correlation function depends not only on C and α, as in transmission, but on z_0 as well. Since α and C

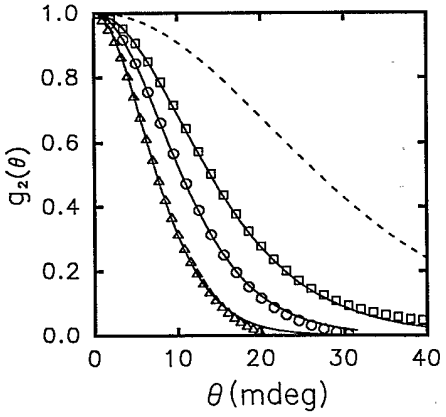

FIG. 4. Correlation functions for alumina samples: □, $L = 0.256$ mm; ○, $L = 0.385$ mm; △, $L = 0.615$ mm. The solid line indicates a fit to Eq. (2.37) with a single set of fitting parameters for all three curves: $C = 0.212$ mm and $\alpha = 0.8$ mm^{-1}. The dashed line is the theory for $L = 0.615$ mm with no reflection or absorption ($C = 0$ and $\alpha = 0$).

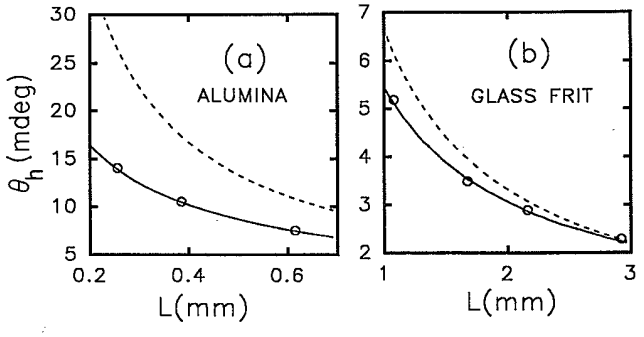

FIG. 5. Half-width θ_h of angular correlation functions obtained in transmission measurements vs sample thickness for (a) alumina and (b) glass frit samples. The solid line in (a) indicates a fit to Eq. (2.37). The dashed line is calcuated from Eq. (2.10) without reflection and absorption. Similar curves are shown in (b) for a glass sample where the effect of internal reflection is smaller due to smaller index mismatch.

are determined from transmission experiments, the measurements of $g_2(\theta)$ in backscattering can be used to determine the remaining unknown parameter z_0. In previous measurements of the temporal autocorrelation functions in multiply scattering colloidal suspensions, and in measurements of the coherent backscattering cone, z_0 was found to be approximately equal to l^* to within $\pm 30\%$. Thus, once z_0 is known, we can exploit this empirical relationship to determine l^*. In Fig. 6 we plot the measured angular autocorrelation functions of the polarized intensity in the backscattering geometry for (a) the alumina sample with $L = 0.615$ mm and (b) the glass frit sample with $L = 2.92$ mm. The solid lines are fits to Eq. (2.40) that give $z_0 = 50$ μm for both samples. By contrast, we show, by the dashed lines the calculation using Eq. (2.40) with $C = 0$, $\alpha = 0$ and $z_0 = 50$ μm. These results decay much more slowly than the data. By using $l^* = 50$ μm for both samples, we obtain $R = 0.73$ for the alumina sample and $R = 0.63$ for the glass frit. These values are substantially higher than the reflection coefficient for normal incidence from air to glass which is 0.04. However, much of the multiply scattered light inside the sample is incident on the boundary at very large angles resulting in total or near total internal reflection. Thus the internal reflection coefficient multiply can be quite high even for moderate index mismatch.

C. Estimation of R from Fresnel's law

We can obtain an estimate of the reflection coefficient R using Fresnel's law. We assume that the direction and polarization of diffusing light incident on the boundary from inside the sample is completely random and that the sample surface is flat. For an angle of incidence θ the reflection coefficient $R(\theta)$ averaged over polarization is

$$R(\theta) \equiv \frac{R_\perp(\theta) + R_\parallel(\theta)}{2} , \tag{3.1}$$

where $R_\perp(\theta)$ and $R_\parallel(\theta)$ are the Fresnel reflection coefficients for incident light polarized perpendicular and parallel to the plane of incidence, respectively [13]. The reflected flux for a given angle of incidence at $z = 0$ is

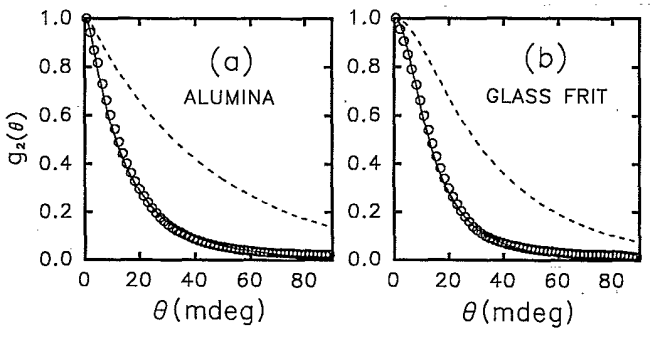

FIG. 6. Correlation functions obtained in backscattering for (a) an alumina sample and (b) a glass frit. The solid lines indicate fits to Eq. (2.40). Both fits give $z_0 = 50$ μm. The dashed lines are calcuated from Eq. (2.40) with $C = 0$, $\alpha = 0$, and $z_0 = 50$ μm.

$R(\theta)J(\theta)$, where $J(\theta)$ is the angle-dependent flux incident on the interface from *inside* the sample. To obtain $J(\theta)$, we consider once again the flux, given by Eq. (2.12), from a volume element dV through an arbitrary small area dS inside the sample. Integrating over r and φ we obtain an expression for $J(\theta)$:

$$J(\theta) = \frac{Uv}{2}\cos\theta + \frac{vl^*}{2}\frac{\partial U}{\partial z}\cos\theta\sin\theta . \tag{3.2}$$

At $z = 0$ the only diffusive flux in the $+z$ direction is from *reflected* light. Thus the total flux in the $+z$ direction at $z = 0$ is obtained by integrating over light reflected through all θ

$$J_+ = \int_0^{\pi/2} d\theta\, J(\theta)R(\theta) . \tag{3.3}$$

Away from the boundary inside the sample, J_+ is given by Eq. (2.17). Within the diffusion approximation, these two expressions for J_+, Eqs. (2.17) and (3.3), must be equal near the sample boundary at $z = 0$. Thus, setting Eqs. (2.17) and (3.3) equal and using the expression for $J(\theta)$ in Eq. (3.2), we obtain the boundary condition at $z = 0$,

$$U - l^*\frac{\frac{1}{3} + C_2}{\frac{1}{2} - C_1}\frac{\partial U}{\partial z} = 0 , \tag{3.4}$$

where

$$C_1 \equiv \int_0^{\pi/2} d\theta R(\theta)\sin\theta\cos\theta \tag{3.5}$$

and

$$C_2 \equiv \int_{-\pi/2}^{0} d\theta R(\theta)\sin\theta\cos^2\theta . \tag{3.6}$$

At $z = L$, we obtain a similar boundary condition,

$$U + l^*\frac{\frac{1}{3} + C_2}{\frac{1}{2} - C_1}\frac{\partial U}{\partial z} = 0 . \tag{3.7}$$

Equations (3.4) and (3.7) have the same form as the boundary conditions we previously derived, Eqs. (2.30) and (2.31), provided we make the identification

$$C = l^*\frac{\frac{1}{3} + C_2}{\frac{1}{2} - C_1} . \tag{3.8}$$

We can obtain an expression for the parameter R, which depends only on the indices of refraction of the sample and the surrounding medium (e.g., air or glass), by comparing Eq. (3.8) with Eq. (2.22). This gives

$$R = \frac{3C_2 + 2C_1}{3C_2 - 2C_1 + 2} . \tag{3.9}$$

Taking $n = 1.7$ for the alumina and $n = 1.5$ for the glass frit we obtain $R = 0.68$ for the alumina sample and $R = 0.57$ for the glass frit. These values are in reasonable agreement with the experimental estimates of 0.73 and 0.63, respectively.

We note that the treatment of reflections given

above differs from the earlier treatment of Lagendijk, Vreeker, and DeVries [3] in that it allows for angle- and polarization-dependent internal reflection of light. Thus we are able to predict the value of the reflection coefficient incorporated into the boundary conditions in terms of known material parameters, namely the indices of refraction of the scattering medium and the sample container. Furthermore, in the absence of internal reflection, we recover boundary conditions which are more consistent with the Milne solution than the perfectly absorbing boundary conditions sometimes used [3, 8].

IV. APPLICATIONS

Since internal reflection of light changes the path length distribution $P(s)$, its effects must be taken into account in measurements of other quantities which involve multiply scattered light. Below, we discuss the effects of internal reflection on dynamic light scattering in the multiple-scattering limit, coherent backscattering, and frequency correlations. Because all of these measurements depend on $P(s)$ in essentially the same way, we can generalize our results for angular correlations to each of these measurements. In fact, in each of these cases we show how the expressions obtained in the absence of internal reflection can be modified to obtain more general expressions which apply when internal reflections are not negligible. Furthermore, in all cases, the effects of internal reflection enter the expressions by means of the same parameter C. Thus, at least in principle, it is possible to determine C, and the effects of internal reflection, from the angular correlation function in transmission, and use this value for other measurements. The angular correlation function in transmission has the unique advantage that, in the absence of absorption, the only other parameter it is dependent on is the sample thickness, which can easily be determined independently. It is this fact which makes the angular correlation function so useful.

A. Diffusing-wave spectroscopy

Diffusing-wave spectroscopy (DWS) is the extension of dynamic light scattering to the multiple-scattering regime and involves the analysis of the temporal fluctuations in the intensity of the light multiply scattered from mobile particles. The normalized intensity correlation function measured experimentally is $\langle I(0)I(\tau)\rangle/\langle I\rangle^2 = 1+\beta|g_1(\tau)|^2$ where β is again a constance which depends on the collection optics. For a suspension of colloidal particles undergoing Brownian motion, the normalized field autocorrelation function $g_1(\tau)$ is given by

$$g_1(\tau) \propto \int_0^\infty P(s)e^{-2(\tau/\tau_0)s/l^*} , \tag{4.1}$$

where τ_0 is the characteristic time for particle motion. For diffusing Brownian particles, $\tau_0 = 1/D_p k^2$ where D_p is the diffusion coefficient of the particles and $k = 2\pi n/\lambda$ is the wave vector of the light in the sample. Equation (4.1) has exactly the same form as the general expression for the angular correlation function with no absorption, except that q is replaced by $\frac{1}{l^*}\sqrt{\frac{6\tau}{\tau_0}}$. Thus, for plane-wave incidence, the form of $g_1(t)$ may be obtained from Eq. (2.37) by making the transformation $q \to \frac{1}{l^*}\sqrt{\frac{6\tau}{\tau_0}}$. For example, in transmission we obtain

$$g_1(\tau) = \frac{L+2C}{z_0+C}\frac{\sinh[(z_0/l^*)\sqrt{6\tau/\tau_0}] + (C/l^*)\sqrt{6\tau/\tau_0}\cosh[(z_0/l^*)\sqrt{6\tau/\tau_0}]}{[1+(C/l^*)^2 6\tau/\tau_0]\sinh[(L/l^*)\sqrt{6\tau/\tau_0}] + (2C/l^*)\sqrt{6\tau/\tau_0}\cosh[(L/l^*)\sqrt{6\tau/\tau_0}]} . \tag{4.2}$$

For $R = 0$, the above equation reduces to the same functional form obtained previously [6].

If experimental data from a DWS measurement are interpreted without including the effects of internal reflection, the value of L/l^* obtained by fitting the data to Eq. (4.2) with $R = 0$ will be somewhat larger than its actual value. Physically, this reflects the increase in the effective path length due to the internal reflection. Thus the value of l^* will be underestimated. For example, with $R = 0.2$ and $L/l^* = 10$, l^* will be underestimated by 10% if internal reflection at the boundaries is not included. Previous reports of DWS measurements in transmission are consistent with these considerions [6].

In the backscattering geometry, the effects of internal reflection on a DWS measurement can be even more pronounced. In previous reports, the autocorrelation function in backscattering for a thick sample ($L \gg l^*$) were found to be well approximated by [11]

$$g_1(\tau) = \exp(-\gamma\sqrt{6\tau/\tau_0}) , \tag{4.3}$$

where γ was observed to be a function of polarization and the ratio l^*/l. Here we emphasize that γ is also a function of the reflection coefficient R. Making the substitution of $q \to \frac{1}{l^*}\sqrt{\frac{6t}{\tau_0}}$ in Eq. (2.41), we obtain an expression for the temporal autocorrelation function with internal reflection

$$g_1(\tau) = \frac{e^{-z_0\sqrt{6\tau/\tau_0}/l^*}}{1+C\sqrt{6\tau/\tau_0}/l^*} . \tag{4.4}$$

Performing a small time expansion of Eqs. (4.3) and (4.4), we obtain the relationship

$$\gamma = \frac{z_0+C}{l^*} = \frac{z_0}{l^*} + \frac{2(1+R)}{3(1-R)} . \tag{4.5}$$

Thus the value of γ can depend on the optical properties of the sample container and its surroundings. For exam-

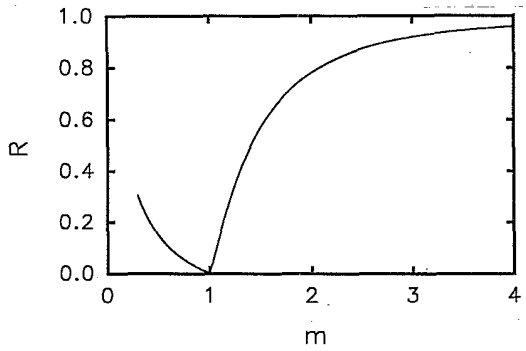

FIG. 7. Calculated reflection coefficient vs index mismatch $m = n_s/n_0$, where n_s is the index of refraction of the sample and n_0 is the index of refraction of the surrounding medium.

ple, for $z_0 = l^*$ and $R = 0$, $\gamma = 1.67$. By contrast, for $R = 0.2$, $\gamma = 2$. Note that finite values of R lead to larger values of γ. In Fig. 7 we show the reflection coefficient as a function of index mismatch.

B. Coherent backscattering

Another commonly performed experiment, which is also strongly affected by internal reflection, is the coherent enhancement of backscattered light [2, 14]. The angular width of the coherent backscattered cone has been used as a direct measure of l^*. The equation for the angular correlation function, Eq. (2.34), has exactly the same form as the expression for the coherent backscattering cone [14]. Thus, for very thick samples, the angular dependence of the coherent backscattering cone is given by Eq. (2.41) and the inverse angular width is given by $[z_0/l^* + 2(1+R)/3(1-R)]k_0 l^*$. Even a modest index mismatch at the sample boundaries can lead to significant corrections to the apparent value of l^* measured using coherent backscattering. For example, a reflection coefficient of $R = 0.2$ increases the value of γ from 1.67 to 2. Thus caution must be exercised in interpreting the width of the coherent backscattering cone, and the effects of internal reflection must be considered.

C. Frequency correlation

Another measurement which can also be strongly affected by internal reflection is the frequency correlation of transmitted light as the incident frequency is changed. Such measurements have been used, for example, to determine the diffusion coefficient D of light [15]. The phase shift of a path of length s due to a frequency shift $\Delta\nu$ is $2\pi s\Delta\nu/v = 2\pi\Delta\nu s l^*/3D$. An expression for the frequency autocorrelation function can be obtained within the diffusion approximation in a fashion analogous to that used to obtain other correlation functions by summing the contribution from all paths. The result is

$$g_1(\Delta\nu) \propto \int_0^\infty P(s) e^{i2\pi\Delta\nu s l^*/3D - s/l_a} ds \,. \tag{4.6}$$

Equation (4.6) has the same form as the general expression for the angular autocorrelation function, Eq. (2.37). Thus explicit expressions for the frequency autocorrelation function for different geometries can be obtained from our formulas for the angular autocorrelaton function by making the substitution $q \to \sqrt{i2\pi\Delta\nu/D}$ into Eqs. (2.37) and (2.40). Once again, the effect of reflections is to increase the effective length of light paths through a sample. Thus, if internal reflection is not taken into account, the apparent diffusion coefficient extracted from a fit to the data will be smaller than its actual value. However, because the effects of internal reflection decrease with increasing sample thickness, the fitted value of D should increase and saturate at the true value when $L \gg C$. These results are consistent with the recent report using microwave measurements [16].

D. Pulse propagation

Internal reflection can also strongly affect pulse propagation and the transmission coefficient of light through random media. For an instantaneous pulse of light incident on a random medium, the transmitted pulse is broadened in time. Physically, this reflects the fact that photons traverse a distribution of path lengths. Those with shortest paths escape from the sample first and those with longer paths escape later. The functional form of the transmitted pulse is simply $P(s)$ with the transformation of variables $s = vt$. For plane-wave incidence, the solution of the diffusion equation is given by Carslaw and Jaeger for the slab geometry [10]

$$P(t) \propto \sum_{m=1}^{\infty} \frac{k_m[\sin(k_m z_0) + Ck_m\cos(k_m z_0)][\cos(k_m L) - Ck_m \sin(k_m L)]}{(C^2k_m^2+1)L + 2C} e^{-D(k_m^2+\alpha^2)t} \,, \tag{4.7}$$

where k_m is mth positive root of the hyperbolic equation

$$\tan(kL) = \frac{2kC}{C^2k^2 - 1} \,, \tag{4.8}$$

$D = vl^*/3$ is the diffusion coefficient of light, and $\alpha^2 = 3/l_a l^*$. The internal reflection increases the path length which delays the peak of transmitted pulse and broadens its width. At long times, where $P(t)$ decays exponentially, the decay is slower when reflection is included. Thus, if internal reflection is not taken into account, the apparent diffusion coefficient extracted from a fit to the data will be smaller than its actual value. For example, fitting the exponentail tail of $P(t)$ by assuming $R = 0$ and renormalizing D gives the apparent diffusion coefficient

$$D^* \approx D\left(1 - \frac{8Rl^*}{3(1-R)L}\right). \tag{4.9}$$

A similar result was obtained by Lagendijk, Vreeker, and DeVries [3], but with a slightly different numerical coefficient resulting from their assuming perfectly absorbing walls in the absence of reflection (see Sec. II B).

V. CONCLUSIONS

We have developed a simple theory to describe the internal reflection of light at the sample boundaries in systems which multiply scatter light. We find that the effects of internal reflection can be accounted for by incorporating a single parameter C into the boundary conditions of the diffusion equation for light. Using these boundary conditions in the solution of the diffusion equation, we obtain explicit expressions for various experimentally measurable quantities, including the angular, temporal, and frequency autocorrelation functions, as well as the coherent backscattering cone and the shape of the transmitted pulse in a pulse propagation experiment.

We find that the measurements of the angular correlation functions are in excellent agreement with the theory only when the effect of internal reflection at the sample interface is properly taken into account. The angular autocorrelation functions depend on sample thickness, absorption, and internal reflection. The effects of reflection and absorption can be independently determined through their different dependences on sample thickness. Internal reflection increases the light path by a fixed amount which depends on the reflection coefficient. Therefore, in transmission experiments, internal reflection is most significant for thin samples. By contrast, absorption cuts off long paths and, therefore, is significant only for transmission through thick samples. Thus measurements of $g_1(q)$ as a function of thickness can be used to determine the absorption and reflection parameters α and C, respectively. To obtain a value for the reflection coefficient R which appears in C, the transport mean free path l^* must be known. An estimate of l^* can be obtained from backscattering measurements of the angular correlation function. Thus, by measuring autocorrelation functions for different thicknesses in both transmission and backscattering, we can determine the absorption parameter and obtain an estimate of the reflection coefficient and the transport mean free path.

Finally, using a simple model based on Fresnel theory, we calculated the dependence of the reflection coefficient on the index mismatch at the sample boundaries. As expected, larger index mismatch leads to larger reflection coefficients. The reflection coefficients we calculate are in good agreement with the measured values of R for samples with different index mismatch. Thus reasonable *a priori* estimates of the effects of reflection are possible for a given experiment using multiple light scattering.

ACKNOWLEDGMENTS

We are grateful to Paul Chaikin and Shechao Feng for useful discussions.

[1] A. Ishimaru, *Wave Propagation and Scattering in Random Media* (Academic, New York, 1978).
[2] *Scattering and Localization of Classical Waves in Random Media*, edited by P. Sheng (World Scientific, Singapore, 1990).
[3] A. Lagendijk, R. Vreeker, and P. DeVries, Phys. Lett. A **136**, 81 (1989).
[4] I. Freund, M. Rosenbluh, and R. Berkovits, Phys. Rev. B **39**, 12403 (1989).
[5] I. Freund, M. Rosenbluh, and R. Berkovits, Phys. Rev. B **41**, 496 (1990).
[6] D.J. Pine, D.A. Weitz, G. Maret, P.E. Wolf, E. Herbolzheimer, and P.M. Chaikin, *Scattering and Localization of Classical Waves in Random Media*, edited by P. Sheng (World Scientific, Singapore, 1990).
[7] D.J. Pine, D.A. Weitz, J. X. Zhu, and E. Herbolzheimer, J. Phys. (Paris) **51**, 2101 (1990).
[8] S. Feng, C. Kane, and A. D. Stone, Phys. Rev. Lett. **61**, 834 (1988).
[9] S. Glasstone and M. C. Edlund, *The Elements of Nuclear Reactor Theory* (Van Nostrand, Princeton, NJ, 1955).
[10] H. S. Carslaw and J. C. Jaeger, *Conduction of Heat in Solids*, 2nd ed. (Clarendon, Oxford, 1990).
[11] D.J. Pine, D.A. Weitz, P.M. Chaikin, and E. Herbolzheimer, Phys. Rev. Lett. **60**, 1134 (1988).
[12] F.C. Mackintosh, J.X. Zhu, D.J. Pine, and D.A. Weitz, Phys. Rev. B **40**, 9342 (1989).
[13] M. Born and E. Wolf, *Principles of Optics*, 4th ed. (Pergamon, New York, 1990).
[14] P.E. Wolf, G. Maret, E. Akkermans, and R. Maynard, J. Phys. (Paris) **49**, 63 (1988).
[15] J.M. Drake and A.Z. Genack, Phys. Rev. Lett. **63**, 259 (1989).
[16] L. A. Ferarri, J. Appl. Phys. **68**, 4399 (1990).